pendicular, have a some what lower ground state and/or higher excited state. On the other hand, the excited state of Cu(c) with two neighboring sulfur atoms, which have their aryl groups parallel, is lower (and/or the ground state is higher) because the electron repulsion is changed into an attracting three-electron sulfur–sulfur bond (see Figure 7). At low temperatures, the excited state in **2** on Cu(b) remains on one side of the complex, whereas the one on Cu(a) stays at the other. At higher temperatures energy transfer occurs which results in localization of the excited state at Cu(b), from where emission occurs.

In $[CuSC_6H_4[(R)\text{-}CH(Me)NMe_2]\text{-}2]_3$ (**1**), the copper atoms are all identical and of the Cu(b) type. The broadness of the spectral bands and the considerable Stokes shift indicates that electron-vibrational coupling is strong. This suggests that the excited state remains localized due to relaxation. The Stokes shift in **2** (9000 cm^{-1}) is somewhat larger than in **1** (7500 cm^{-1}). This might be explained by a delocalization of the hole in excited **1** via the lone electron pair orbital of the third sulfur which has the right symmetry to form a five-electron three sulfur center bond. This, in turn, results in a less outspoken relaxation around the central copper atom, so that the Stokes shift is also less.

From this we conclude that the excited state is not delocalized over the Cu_3 unit or the aromatic rings. Murphy et al. have recently reported room temperature luminescence from tetrametallic complexes of ruthenium.[35] They ascribed this to localization of the MLCT transition involved. This runs parallel to our view. The competition between localization and delocalization has been discussed by one of us elsewhere.[36] Other examples are localization of the chromate tetrahedra[37] and the localization in the different molybdate groups in $MgMoO_4$.[38]

Contribution from the Department of Chemistry and Materials Science Center, Cornell University, Ithaca, New York 14853, and AT&T Bell Laboratories, Murray Hill, New Jersey 07974

Relationships between Extended Structures and Molecular Clusters of Nickel and Tellurium

Zafiria Nomikou,[†] Boris Schubert,[†] Roald Hoffmann,*[,†] and M. L. Steigerwald[‡]

Received July 24, 1991

The synthesis of bulk NiTe from molecular precursors of the zero-valent elements under very mild conditions was previously reported. In that study, two molecular intermediate clusters, $Ni_9Te_6(PEt_3)_8$ and $Ni_{20}Te_{18}(PEt_3)_{12}$ were also isolated. Consequently, the idea of structurally relating the molecules to the solid emerged. In this work we relate a cut, extracted from the solid NiTe, to each of the two clusters. The structural relation of the smaller cluster to the bulk is very clear; extended Hückel calculations actually favor a geometry between the observed cluster structure and hypothetical cut from the solid. The bigger cluster, although apparently complex and intricate, is also derivable from the bulk, if one includes two interstitial Ni atoms, as found in a related Ni_2In structure.

The preparation of extended atomic arrays in the solid state from molecular precursors has been much developed within the last decade. This approach allows higher reaction rates and hence lower temperatures than the classic ceramic preparative routes. In this context, Steigerwald and co-workers[1] were seeking an advantageous technique to prepare large intermetallic clusters. They decided to synthesize the solid-state compound nickel telluride, NiTe, using organometallic complexes of zero-valent tellurium and nickel, in particular, bis(cyclooctadiene)nickel ($Ni(COD)_2$) and $TePR_3$.[2] They isolated and crystallographically characterized two intermediate clusters, $Ni_9Te_6(PEt_3)_8$ (**1**) and $Ni_{20}Te_{18}(PEt_3)_{12}$ (**2**).

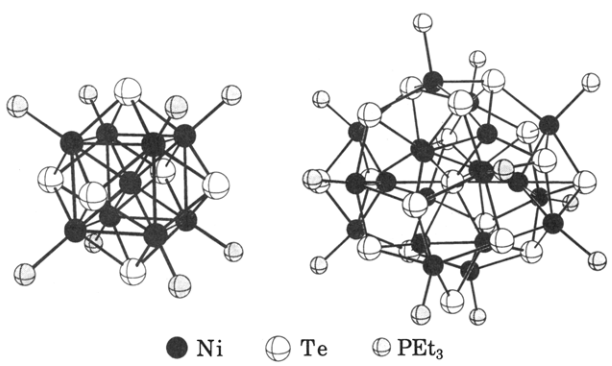

1 **2**

In this paper we (1) show that **1** and **2** each bear a simple structural relationship to the NiTe extended solid; (2) show paths along which the structures of the clusters can be deformed to give direct, excised fragments of NiTe; and (3) show, using model calculations of the extended Hückel type, the energy trends associated with the cluster to fragment distortion. These latter calculations indicate that the crystallographically determined structure of **1** is perhaps not the lowest enthalpy geometry of $L_8Ni_9Te_6$ (L = two electron donor ligand).

The idea that solid-state structures and discrete molecular clusters are related is hardly new; many researchers have suggested that clusters[3] may play an intermediary role in the routes to larger metal complexes and solid-state materials.[4] In particular, clusters

[†] Cornell University.
[‡] AT&T Bell Laboratories.

(1) (a) Steigerwald, M. L.; Brus, L. E. *Annu. Rev. Mater. Sci.* **1989**, *19*, 471. (b) Brennan, J. G.; Siegrist, T.; Carroll, P. J.; Stuczynski, S. M.; Brus, L. E.; Steigerwald, M. L. *J. Am. Chem. Soc.* **1989**, *111*, 4141. (c) Steigerwald, M. L.; Sprinkle, C. R. *Organometallics* **1988**, *7*, 245.
(2) Brennan, J. G.; Siegrist, T.; Stuczynski, S. M.; Steigerwald, M. L. *J. Am. Chem. Soc.* **1989**, *111*, 9240.
(3) (a) Mingos, D. M. P.; Wales, D. J. *Introduction to Cluster Chemistry*; Prentice Hall: Englewood Cliffs, NJ, 1990. (b) *The Chemistry of Metal Cluster Complexes*; Shriver, D. F., Kaesz, H. D., Adams, R. D., Eds.; VCH: New York, 1990. (c) *Metal Clusters*; Moskovits, M., Ed.; Wiley-Interscience, J. Wiley & Sons: New York, 1986. (d) *Metal Clusters in Catalysis*; Gates, B. C., Guczi, L., Knözinger, H., Eds.; Studies in Surface Science and Catalysis 29; Elsevier: Amsterdam, 1986. (e) *Metal Clusters in Chemistry*; Lewis, J., F. R. S., Green, M. L. H., Eds.; Royal Society: London, 1982. (f) *Transition Metal Chemistry*; Müller, A., Diemann, E., Eds.; Verlag Chemie: Weinheim, Germany, 1981. (g) Johnson, B. F. G.; Lewis, J. In *Advances in Inorganic Chemistry and Radiochemistry*; Emeléus, H. J., Sharpe, A. G., Eds.; Academic Press: New York, 1981; Vol. 24, pp 225–355. (h) Simon, A. *Angew. Chem.* **1988**, *100*, 163; *Angew. Chem., Int. Ed. Engl.* **1988**, *27*, 159. (i) von Schnering, H. G. *Angew. Chem.* **1981**, *93*, 44; *Angew. Chem., Int. Ed. Engl.* **1981**, *20*, 33. (j) Simon, A. *Angew. Chem.* **1981**, *93*, 23; *Angew. Chem., Int. Ed. Engl.* **1981**, *20*, 1. (k) Schäfer, H.; Schnering, H. G. *Angew Chem.* **1964**, *76*, 833.

0020-1669/92/1331-2201$03.00/0 © 1992 American Chemical Society

analogous to the smaller $Ni_9Te_6(PEt_3)_8$ molecule have been prepared by Fenske and co-workers as well as others.[5]

It is interesting to trace relationships between the molecular clusters and the solid. We will try to construct a pathway that will link a piece, conveniently cut from the solid NiTe, to each of the reported clusters **1** and **2**. We hope that in doing so we will be able to not only rationalize the formation and stability of the clusters but also appreciate the development of the structure and properties of the extended solid with particle size.

In the NiTe system there have been no less than five different phases reported.[6] For a Ni to Te ratio of 1:1 the solid crystallizes in the so-called δ-phase, in which it assumes the NiAs structure **3**.[6,7] In this structure, tellurium atoms form hexagonal close-

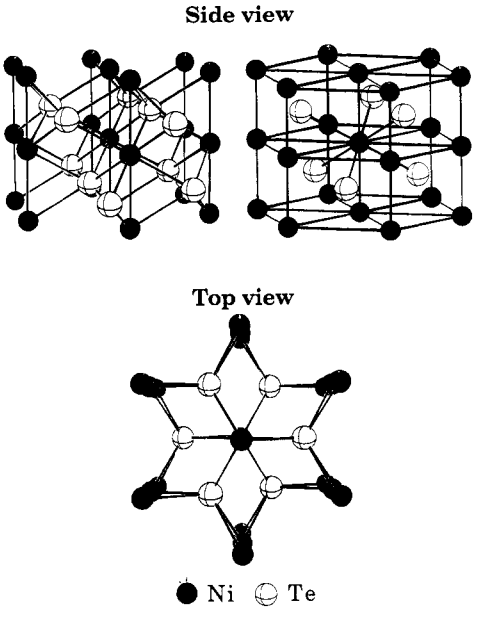

3

packed layers and nickel atoms fill the octahedral holes. The Ni atoms thus form a trigonal prismatic environment around each Te, while themselves lying in hexagonal planar nets. Each $NiTe_6$ octahedron (Ni–Te 2.65 Å) shares a pair of opposite faces with adjacent octahedra, thus bringing two Ni atoms, one from each nearest hexagonal layer, to a bonding distance of 2.68 Å. The intralayer Ni–Ni distance is long, 3.97 Å. We will relate the structures of **1** and **2** to this extended solid structure.

$Ni_9Te_6(PEt_3)_8$

The Ni_9Te_6 core of the cluster is shown in **4**. It consists of a central Ni atom (Ni1) surrounded by a cube of eight Ni atoms (Ni2 and Ni3). Each face of the Ni cube is capped with a Te atom, the six thereby forming an octahedron. One of the body diagonals of the cube is slightly elongated—thus the crystallo-

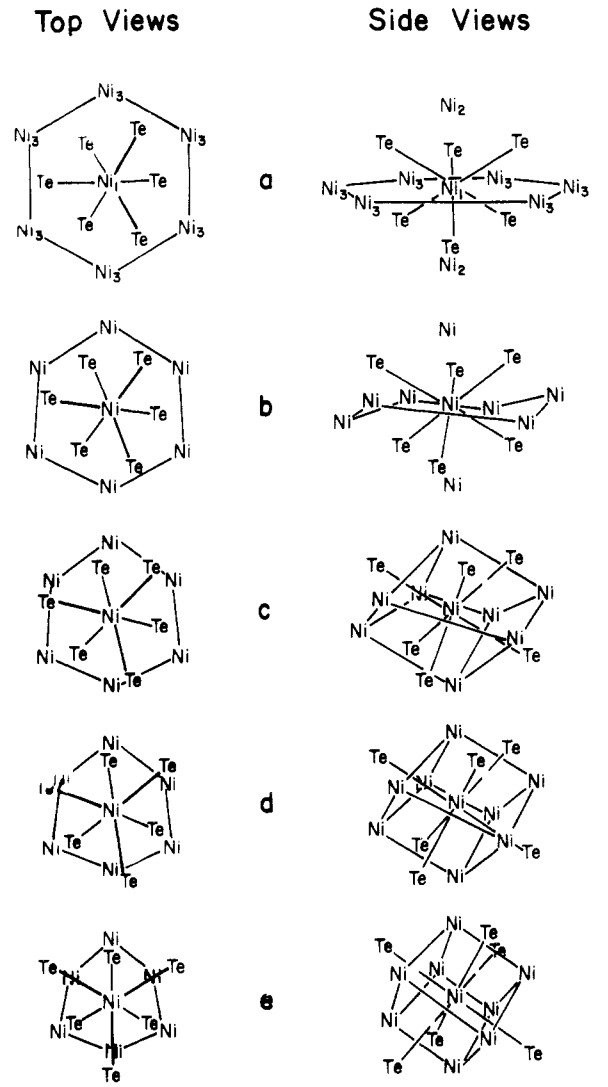

Figure 1. Top and side views of the five-step transit from the cut **a** to the cluster **e** of the Ni_9Te_6 fragment.

graphically distinguishability of Ni2 and Ni3. For comparison in **5** we shown an excised fragment of the NiTe structure: a Ni atom plus its nearest neighbors (six Te atoms) and next nearest neighbors (eight Ni atoms).

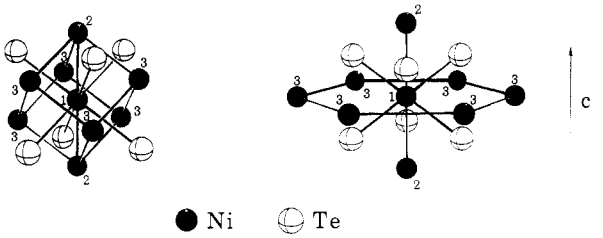

4 **5**

We recognize the first similarity with bulk NiTe by noting that in the cluster Ni1 is surrounded by an octahedron of Te atoms, although the Ni–Te distance of 2.98 Å is longer than in the bulk (2.65 Å).

If we take a look at the extended NiTe structure along the *c* direction, that perpendicular to its hexagonal layers, we notice that the six Te atoms around a Ni atom form a distorted octahedron. Here we recognize the first similarity with the cluster by assigning this nickel atom as Ni1.

In order to study the relationship between **1** and NiTe quantitatively, we must add two-electron ligands to **4** and **5**. As a first model, we attach a H^- ligand bonded radially outward to each one of the eight external Ni atoms at a Ni–H distance of 1.60 Å, a reasonable M–H distance.[8] We have before us a model

(4) (a) Basset, J. M.; Ugo, R. In *Aspects of Homogeneous Catalysis*; Ugo, R., Ed.; D. Reidel: Dordrecht, The Netherlands, 1977; Vol. 3, Chapter 2. (b) Bjørnholm, S. *Contemp. Phys.* **1990**, *31*, 309. (c) Lee, S. C.; Holm, R. H. *Angew. Chem.* **1990**, *102*, 868; *Angew. Chem., Int. Ed. Engl.* **1990**, *29*, 840. (d) Teo, B. K.; Keating, K.; Kao, Y.-H.; *J. Am. Chem. Soc.* **1987**, *109*, 3494. (e) Brus, L. *J. Phys. Chem.* **1986**, *90*, 2555.

(5) (a) Fenske, D.; Ohmer, J.; Hachgenei, J.; Merzweiler, K. *Angew. Chem.* **1988**, *100*, 1300; *Angew. Chem., Int. Ed. Engl.* **1988**, *27*, 1277, and references therein. (b) Fenske, D.; Merzweiler, K.; Ohmer, J. *Angew. Chem.* **1988**, *100*, 1572; *Angew. Chem., Int. Ed. Engl.* **1988**, *27*, 1512. (c) Fenske, D.; Hollnagel, A. *Angew. Chem.* **1989**, *101*, 1412; *Angew. Chem., Int. Ed. Engl.* **1989**, *28*, 1390. (d) Fenske, D.; Fleischer, H.; Persau, C. *Angew. Chem.* **1989**, *101*, 1740; *Angew. Chem., Int. Ed. Engl.* **1989**, *28*, 1665. (e) Fenske, D.; Krautscheid, H. *Angew. Chem.* **1990**, *102*, 1513; *Angew. Chem., Int. Ed. Engl.* **1990**, *29*, 1452. (f) Hong, M.; Huang, Z.; Liu, H. *J. Chem. Soc., Chem. Commun.* **1990**, 1210.

(6) Barstad, J.; Grønvold, F.; Røst, E.; Vestersjø, E. *Acta Chem. Scand.* **1966**, *20*, 2865.

(7) Wells, A. F. *Structural Inorganic Chemistry*, 5th ed.; Clarendon: Oxford, UK, 1984; Chapter 17, p 753.

Table I. Calculational Results for the Model Steps **a**–**e**

steps	a[a]	b	c	d	e[b]
total overlap populatns					
Ni1–Te	1.728	1.236	0.972	0.750	0.480
Ni2–Te	1.806	2.100	2.148	2.160	2.196
Ni3–Te	4.140	5.844	6.546	6.438	6.286
total Ni–Te	7.674	9.180	9.666	9.348	8.962
shortest dist Ni–Te, Å	2.655	2.418	2.333	2.389	2.545
total overlap populatns					
Ni1–Ni2	0.080	0.120	0.152	0.174	0.194
Ni1–Ni3	−0.030	−0.018	0.018	0.138	0.446
Ni2–Ni3	0.000	−0.012	−0.018	−0.012	0.060
Ni3–Ni3	−0.006	−0.018	−0.030	0.006	0.030
total Ni–Ni	0.044	0.072	0.122	0.306	0.730
shortest dist Ni–Ni, Å	2.681	2.628	2.574	2.521	2.467
total overlap populatns					
Te–Te	0.468	0.315	0.135	0.051	−0.042
shortest dist Te–Te, Å	3.527	3.693	3.863	4.037	4.215
rel total energy, eV	0.00	−4.20	−4.65	−2.20	0.39

[a] Cut. [b] Cluster.

$Ni_9(\mu_4\text{-}Te)_6L_8$ ($L = H^-$, PR_3) molecule, which we will from this point on call the "cut" (cut from the solid), **5**, and related to it, the symmetrized cluster **4**, whose geometry is very close to that of **1**. These will in fact define stages **a** and **e**, respectively, in a hypothetical smooth five-stage transit from the cut to the cluster, illustrated in Figure 1.[9]

During this transition the only atom which remains fixed is Ni1. The six telluriums, initially at 2.65 Å from Ni1, move away from it, reaching the final Ni1–Te distance of 2.98 Å. At the same time they approach the Ni2–Ni1–Ni2 line along *c*, which in turn will become one of the body diagonals of the nickel cube. This second component of the tellurium motion imitates the closing of an umbrella. There is a third component in the motion of the Te atoms. As shown in the top views in Figure 1, the tellurium atoms rotate around the Ni2–Ni1–Ni2 axis until each Te eclipses a Ni3 atom.

One would guess that during this transition the nickel to tellurium bonds become stronger, as almost all Ni2–Te and Ni3–Te distances decrease. This is true since the Ni–Te interactions are attractive for our particular number of valence electrons. On the other hand, all Ni1–Te bond distances increase. We list a selection of overlap populations calculated along the transit in Table I. The listed values are a simple sum of overlap population values of all bonds of the type specified. Note the decreasing overlap population values of the central nickel atom Ni1 to all the Te atoms as we pass from **a** to **e**. This is expected, as the six Ni1–Te bond distances increase from 2.65 to 2.98 Å. In contrast, the total of the Ni2–Te overlap population values increases from **a** all the way to **e** as the Ni2–Te contacts decrease from 2.655 Å in the solid to 2.545 Å in the cluster. The simply summed total of the Ni3–Te overlap population values, though, initially increases in passing from **a** to **b** and from **b** to **c** and decreases from **c** to **d** and finally from **d** to **e**. Comparing the values of total overlap populations of all Ni1–Te, Ni2–Te, and Ni3–Te bonds, we conclude that Ni–Te bonding is indeed stronger in the cluster than in the extended solid.

The two Ni2 atoms above and below Ni1, initially at a distance of 2.68 Å from it, approach Ni1 during the transition without departing from the vertical Ni2–Ni1–Ni2 line. These axial nickels reach a separation of 2.47 Å from Ni1, forming two of the eight vertices of the resulting nickel cube. In Table I we list the Ni1–Ni2 overlap populations for the different configurations along our passage from **a** to **e**. We notice that these bond strength indicators increase weakly but distinctively. The small absolute values of Ni1–Ni2 overlap populations are characteristic of most metal–metal bonds.

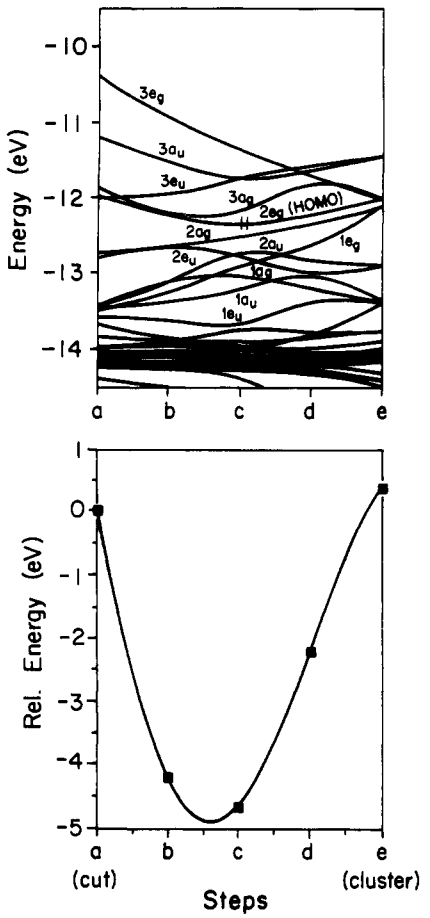

Figure 2. Walsh diagram and relative total energy variation along the five-step transit of the $Ni_9Te_6H_8^{8-}$ model fragment. The highest occupied level is the $2e_g$ set.

The most drastic motions in the cut to cluster transit are executed by the last six nickels, the ones originating in the hexagonal plane of Ni1 in our initial cut. These nickel atoms approach the central nickel from their original separation of 3.97 Å to the final Ni1–Ni3 distance of 2.47 Å. At the same time, they move alternatetly below and above the original horizontal hexagonal plane. Initially at an angle of 90° from the Ni2–Ni1–Ni2 axis, the Ni3's end up at an angle of ±70.5°, without departing from their radical vertical plane.

In our calculations, the Ni1–Ni3 overlap populations increase faster than the Ni1–Ni2 ones, as indicated in Table I. This is because these metal atoms were initially quite far away from the central nickel atom, minimally antibonding. They end up at a bonding distance of 2.47 Å with an overlap population for each Ni1–Ni2 contact of 0.074. In the structure of pure metallic Ni, the nearest neighbor distance is 2.49 Å[10] and the corresponding overlap population is 0.089.

The molecular orbitals (MO's) of a cluster of nine metal atoms are not simple, even in high symmetry. An excellent construction of the MO's of the cluster was recently presented by Wheeler.[11] We obtain the same orbitals. The HOMO consists of a t_{2g}, triply degenerate set, which decomposes into an a_g and an e_g set during the S_6 transit.[12]

In Figure 2 we show a portion of the Walsh diagram along the cut to cluster transit (limiting ourselves to the orbitals near the HOMO–LUMO gap) and the variation of the total energy during

(8) Ibers, J. A. In *Transition Metal Hydrides*; Bau, R., Ed.; American Chemical Society: Washington, DC, 1978; Chapter 3.

(9) During the transition from the cut to the cluster our collection of atoms moves while conserving a C_3 rotation axis and a center of symmetry i. Hence, the molecule remains in point group S_6.

(10) (a) Kohlhaas, R.; Dünner, Ph.; Schmitz-Pranghe, N. *Z. Angew. Phys.* **1967**, *23*, 245. (b) Kantola, M.; Tokola, E. *Ann. Acad. Sci. Fenn., Ser. A6* **1967**, *223*, 1.

(11) Wheeler, R. A. *J. Am. Chem. Soc.* **1990**, *112*, 8737.

(12) Note the degeneracies appropriate to cubic symmetry appearing in the cluster geometry (step **e**) in Figure 2.

this transition. Our semiempirical method of calculation does not give us a minimum in the potential energy curve where we expected it, in the region of the observed cluster. Instead, the lowest energy configuration is one between **b** and **c**, i.e., roughly half-way between cut and cluster.

The first thought that occurs is that the instability of the cluster is due to the unrealistic terminal ligands, H^-, in the model instead of PR_3. We then carried out the calculation with $L = PH_3$ instead of H^- and obtained similar results. A second thought was that this anomaly is a consequence of a poor choice of Ni or Te parameters or of both. However, a wide range of parameters does not alter the computational result that an intermediate geometry is more stable than either cut or cluster. It could still be that we are dealing with a basic failure of the extended Hückel method. But the sum of our experience inclines us to think that there may be something real here—it would be interesting to see if similar clusters with different phosphines (so far unmakable) would retain the cluster geometry or possibly distort in the direction of the cut.

Two different sets of levels seem to be responsible for the rise in energy in the last two steps of the transit—the $2a_g$ and the doubly degenerate $1e_g$ set (see Figure 2). The former level is a molecular orbital of $3d_{z^2}$ character on Ni1 and Ni2 combined in an antibonding way. It also contains $3d_{z^2}$Ni1–$5p_z$Te and $3d_{z^2}$Ni2–$5p_z$Te antibonding combinations. The most important feature of this $2a_g$ level, however, is its Te–Te bonding character, which weakens on going from cut to cluster. As an illustration, the energy of this MO increases by about 0.6 eV.

As we may see in Table I, along the transition the total Te–Te bonding drops. The net interaction even becomes antibonding. The MO mostly responsible for this is the $2a_g$ level. The contribution of Te in $2a_g$ increases from 19.8 to 54.4%. To confirm this, we evaluated the sum total of the various Te–Te overlap populations in this one MO along the transition and found that, from a weakly bonding value of 0.036 for the cut, the sum gradually drops to zero for stage **d** and then becomes antibonding, −0.052, for the cluster, stage **e**. For a calibration we may look at tellurium in its elemental form, stable at atmospheric pressure. Tellurium crystallizes in a helixlike structure, in which there are two Te–Te bonds per Te atom, of 2.84 Å (overlap population 0.468) and four longer Te–Te contacts of 3.50 Å (overlap population −0.005).

We should add here that the quickly growing Ni1–Ni3 antibonding character is also responsible, if to a lesser extent, for the aforementioned destabilization of $2a_g$. This destabilization picks up quickly during the transition, as the Ni1–Ni3 distance decreases from 3.969 to 2.467 Å and the Ni3 composition increases from 3.0 to 28.8%.

The energy variation of the $1e_g$ levels is more dramatic; these two degenerate MO's rise 1.4 eV during the **a**–**e** transit. Originating at −13.5 eV in the cut, the $1e_g$ levels are mainly of 3d character on Ni1 and on all six Ni3 atoms, strongly Ni3–Ni3 antibonding and to a lesser extent Ni1–Ni3 antibonding. While the nickel character decreases in the $1e_g$ levels with the transition, the Ni–Ni antibonding interactions increase from zero to −0.076 for Ni3–Ni3, and from zero to −0.012 for Ni1–Ni3 contacts. This is a result of the dominant shortening of all Ni–Ni bond lengths.

Finally, we comment on the magnetic properties of this compound. Schneemeyer et al.[13] measured the magnetic susceptibility of $Ni_9Te_6(PEt_3)_8$ as a function of temperature. Their data indicate a distinct change in the effective magnetic moment at 80–100 K, with $\mu_{eff}(T<80K) = 4.02\mu_B$ and $\mu_{eff}(T>100K) = 6.08\mu_B$. Using our $[Ni_9(\mu_4\text{-}Te_6)H_8]^{8-}$ model, we calculated a HOMO–LUMO gap of almost zero separating a t_{2g} HOMO, populated with four electrons, from an e_g LUMO. Therefore a range of spin states is accessible to the cluster.

The ordering of the levels near the HOMO–LUMO gap is a sensitive function of the terminal ligands, as also found by Wheeler.[11] With PH_3 ligands the gap is 0.129 eV, but there is a switch in level ordering. Now the e_g orbitals are below the t_{2g} set. Thus the HOMO's (e_g set) are fully occupied (see Figure 3) in a hypothetical low-spin configuration.

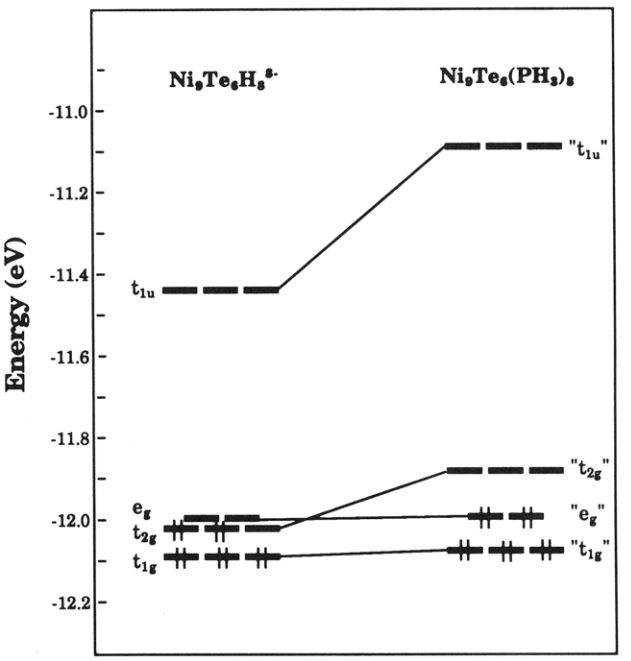

Figure 3. Correlation of the molecular orbitals of the Ni_9Te_6 cluster near the HOMO–LUMO gap with two different sets of ligands: H^-'s (left) and PH_3's (right).

Since the levels near the "Fermi level" of the cluster are so closely spaced and their energies such sensitive functions of ligand, we are tempted to speculate that the high-temperature state ($\mu_{eff} = 6.08\mu_B$) is an enthalpically excited state and that it is only below 80 K that the entropic contribution to the free energy is insignificant, leading to the ground state having $\mu_{eff} = 4.02\mu_B$. The geometrical ramifications of the change in electronic state are interesting and await further study.[14]

$Ni_{20}Te_{18}(PEt_3)_{12}$

This cluster, although very bulky, is not the biggest nickel chalcogenide cluster ever synthesized. There are bigger ones decorating the literature. The one with the biggest nickel matrix in it is probably $Ni_{34}Se_{22}(PPh_3)_{10}$,[15] but by the time this paper is published that record is likely to be surpassed.

$Ni_{20}Te_{18}(PEt_3)_{12}$, shown again in **6**, contains much local symmetry. In the center of it there is a tellurium atom, Te_c, whereas

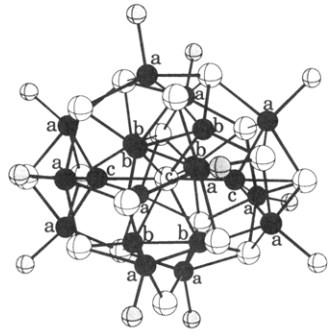

6

the other 17 telluriums are spread over the surface of the cluster.

(13) Schneemeyer, L. F.; Waszczak, J. V.; Palstra, T.; Gyorgy, E. M.; Ramirez, A.; Steigerwald, M. L., manuscript in preparation.

(14) See, for example: (a) Gallois, B.; Real, J.-A.; Hauw, C.; Zarembowitch, J. *Inorg. Chem.* **1990**, *29*, 1152. (b) König, E. In *Progress in Inorganic Chemistry*; Lippard, S. J., Ed.; John Wiley & Sons: New York, 1987; Vol. 35, pp 527–622. (c) König, E.; Ritter, G.; Kulshreshtha, S. K. *Chem. Rev.* **1985**, *85*, 219. (d) Imoto, H.; Simon, A. *Inorg. Chem.* **1982**, *21*, 308.

(15) Fenske, D.; Ohmer, J.; Hachgenei, J. *Angew. Chem.* **1985**, *97*, 993; *Angew. Chem., Int. Ed. Engl.* **1985**, *24*, 993.

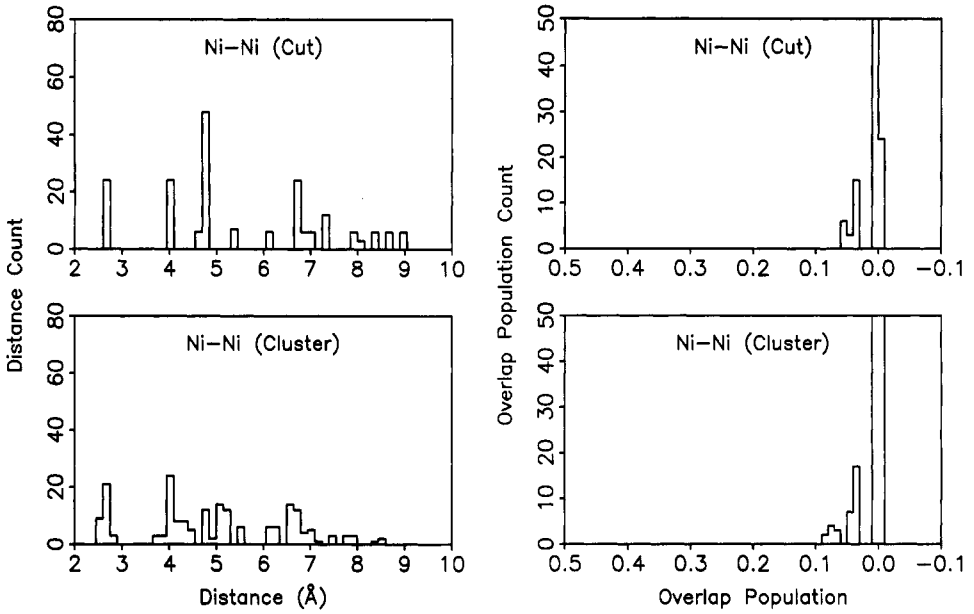

Figure 4. Distribution of Ni–Ni separations and of their associated reduced overlap populations in the cut and cluster models of the $Ni_{20}Te_{18}$ fragment. The number of Ni–Ni reduced overlap populations near zero for both configurations is very large, off scale in these graphs. We chose to truncate the peak around zero overlap population since such values do not contribute to the stability of the two systems.

There are also 20 nickel atoms which we sort into three categories, according to the number of tellurium atoms they are connected to (at a distance range of 2.4–3.0 Å): 12 Ni atoms on the surface of the cluster, labeled as Ni_a in **6**, 6 inner ones, labeled as Ni_b, and the remaining 2, labeled as Ni_c. Finally, there are 12 PEt_3 ligands.

Each Ni_a atom has a square-pyramidal coordination environment. The Ni_a–Te distances are in the range of 2.55–2.69 Å. Each Ni_b atom is pseudotetrahedrally coordinated to four Te atoms at distances of 2.45–2.64 Å. Each of the two Ni_c atoms has a coordination environment of a much distorted trigonal bipyramid, with two short (2.52–2.59 Å) and three long (2.8–2.9 Å) Ni_c–Te distances per Ni_c atom. The short Ni_c–Te contacts occur in the almost linear Te–Ni_c–Te_c–Ni_c–Te array. There are also Ni–Ni bonds in the cluster with bond lengths of 2.45–2.75 Å, as well as Te–Te contacts which might be weakly bonding, in the 3.26–3.84-Å range.

We seek a possible relationship between the cluster and a piece appropriately cut from the extended solid. At first, the combination of the Ni-centered polyhedra in $Ni_{20}Te_{18}(PEt_3)_{12}$ seemed absolutly random. Our initial thought was to determine the underlying symmetry of the cluster. Maybe a hypothetical transition from an appropriate "cut" to this cluster might make use of a relatively high symmetry point group, as in the $Ni_9Te_6(PEt_3)_8$ case.

The almost linaer Te–Ni_c–Te_c–Ni_c–Te array was the most attractive starting point. We plotted a view of the $Ni_{20}Te_{18}(PEt_3)_{12}$ cluster, (omitting the ligands for clarity) looking down the Te–Ni_c–Te_c–Ni_c–Te axis, **7**.

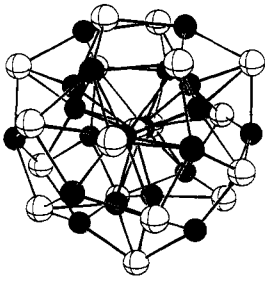

● Ni ⊖ Te

7

That this line is close to being a C_3 axis may be seen by isolating the Ni atoms. We plotted this subset of all the nickels at their intact positions in the cluster, looking down the same Te–Ni_c–Te_c–Ni_c–Te line. This is shown in **8**, where we connect any Ni

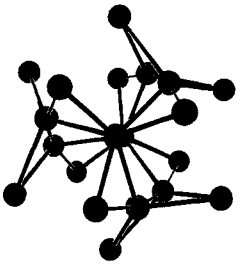

● Ni

8

atoms at distances of ≤2.76 Å. The whole assembly resembles an intricate pattern of a somewhat tipsy propeller. From **8** it becomes apparent that not only is there an approximate C_3 symmetry rotation axis but there are also three 2-fold rotation axes, perpendicular to the C_3. Idealized, the nickel subset of the cluster has at least the symmetry of the D_3 point group.

Recall now the structure of the extended NiTe solid, **3**. It consists of alternate hexagonal, parallel layers of Ni and Te atoms. The site symmetry at Ni atoms is D_{3d}, and at Te atoms, all the symmetry elements of the point group D_{3h} are satisfied. Coming back to the cluster, we redrew the subset of Ni atoms in the cluster, connecting any atoms that were close to lying in the same triangular plane. In **9** we show a top and a side view of the resulting

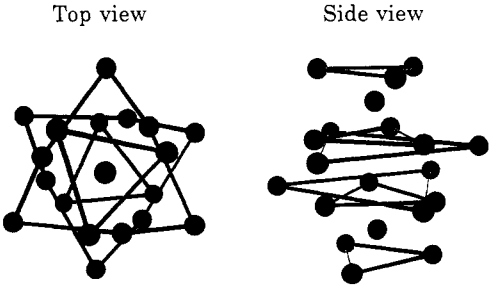

● Ni

9

picture. We notice that the nickels form almost parallel triangular

layers, except for two Ni atoms that are lying between these layers. These solitary atoms would lie along the C_3 axis, which, in turn, would pass through the center of each triangular plane.

The $Ni_{20}Te_{18}(PEt_3)_{12}$ cluster is totally devoid of symmetry, but it may be brought into a geometry of some symmetry. We will approach its idealized configuration by assuming that the nickel atoms form four parallel, triangular layers. The two end triangular layers consist of three Ni atoms each, and the two intermediate layers of six Ni atoms each. Between the centers of the first and second layers, from both the top and the bottom (in the side view), there lie two single Ni atoms. These solitary Ni atoms are of the Ni_c type. Looking at the top view of the real cluster, in **10**, we

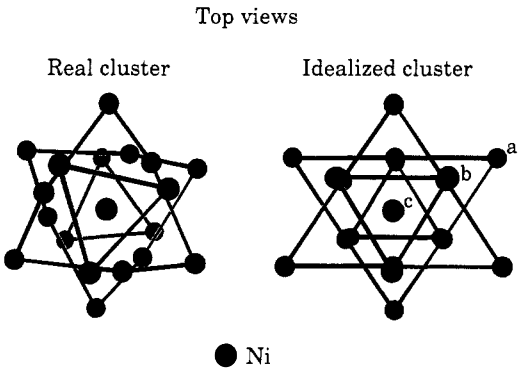

10

notice that the successive nickel triangles cannot be described as either strictly staggered or perfectly eclipsed, but somewhere in between. We choose to consider them as twisted away from a successively staggered ideal. On the right side of **10** we show the hypothetical ideal staggered layering of the Ni atoms. The apices of every triangle, 12 of them, are the Ni_a-type nickels. The remaining six nickel atoms, those that ideally would lie in the middle of every side of the two intermediate triangular layers, are of the Ni_b type.

Next, we included the Te atoms in the picture. There is no implication of Te–Te bonding in these constructions, though we drew lines connecting Te's in triangles. In **11** we show both a top

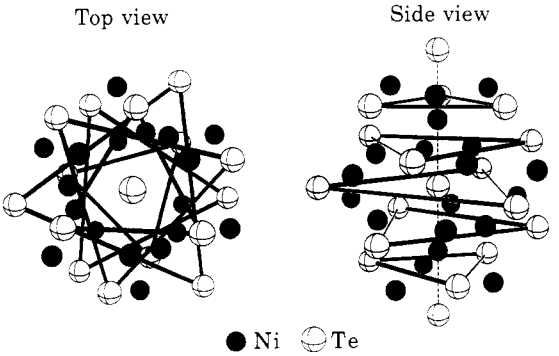

11

and a side view. Again, it seems that an idealized cluster model would consist of five, staggered, triangular, parallel planes. Along the line connecting their centers there would lie a single Te atom in the center, Te_c, and two more Te atoms, capping the outer triangular planes (top and bottom ones in the side view of **11**).

The middle layer would include the three 2-fold rotation axes we assumed when we discussed the nickel subset of the cluster. Each C_2 axis would pass through an apex and the central tellurium, Te_c, of this triangular middle layer. So it seems that that symmetry point group D_3 is still satisfied, even with the inclusion of the telluriums.

So far, we have been able to identify that in a hypothetical, ideal model of the $Ni_{20}Te_{18}(PEt_3)_{12}$ cluster, very similar to the real one, tellurium and nickel atoms alternately lie in triangular layers of their own, around a central C_3 axis. Ni atoms form four such layers, whereas telluriums form five layers, each consisting of three atoms.

Let us now concentrate on the NiTe structure in the solid state. Unlike the Ni_9 cluster case, where we began by focusing on a central Ni, we now concentrate on a Te atom, Te_c, and isolate its six nearest neighbors, as well as its three next nearest neighbors, from the same tellurium layer. Next, we isolate three Te atoms from each of the adjacent tellurium layers, above and below the first one. The Te atoms in these layers form triangles, strictly staggered with respect to the telluriums in the first, central hexagonal plane, as telluriums pack in a BCBC... fashion in NiTe.

So far we have assembled $1 + 6 + 3 + (2 \times 3) = 16$ Te atoms. We satisfy our need for 18 telluriums by including in the picture 1 atom from each next nearest tellurium layer. These last Te atoms lie on the same c axis of the solid with the previously assigned centering Te_c atom. **12** shows the subset of Te atoms we just isolated from the extended NiTe solid.

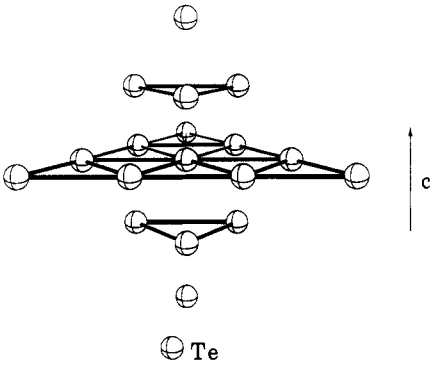

12

The Te atoms are assembled from five successive layers from the solid. In the solid there are four hexagonal layers of Ni atoms lying between them. From these layers it is easy to pick out 18 nickels, shown in **13**, to go with the telluriums we have already chosen. The Te and Ni sublattices are combined in **14**.

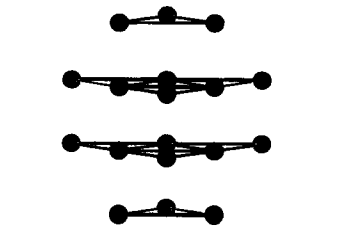

13

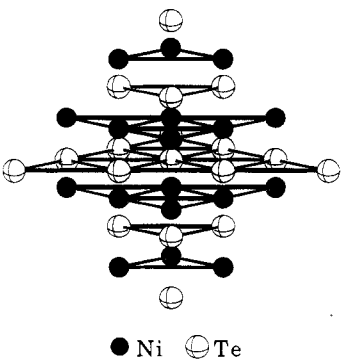

14

At this point we are two nickel atoms short of the cluster stoichiometry. These two atoms must be added along the axis, generating the Te–Ni–Te–Ni–Te line. No such line of five atoms exists in the NiAs structure type. A clue is provided by the Ni_2In structure.[16] This is a "filled" NiAs structure, in the following

(16) Pearson, W. B. *The Crystal Chemistry and Physics of Metals and Alloys*; Wiley-Interscience: New York, 1972; pp 530–531.

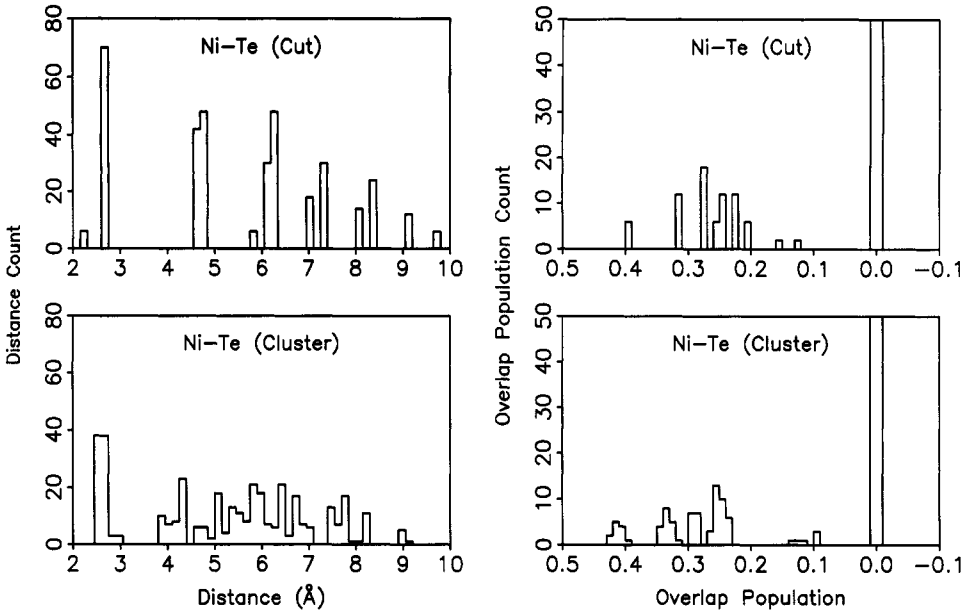

Figure 5. Distribution of Ni–Te separations and of their associated reduced overlap populations in the cut and cluster models of the $Ni_{20}Te_{18}$ fragment. The number of Ni–Te reduced overlap populations near zero for both configurations is very large, off scale in these graphs. We chose to truncate the peak around zero overlap population since such values do not contribute to the stability of the two systems.

sense. There are two types of Ni atoms. Ni(1) atoms form trigonal prisms surrounding the indium atoms. Half of these trigonal prisms are centered by the In atoms and the other half of them are centered by Ni(2) atoms, resulting in a Ni:In atomic ratio of 2:1.

Turning to our cut, **14**, extracted from the solid NiTe, we insert a Ni atom into the center of the next outermost triangular layer. The new positions the two Ni atoms assume coincide with the centers of a trigonal prism of Ni atoms, as shown in **15**. The

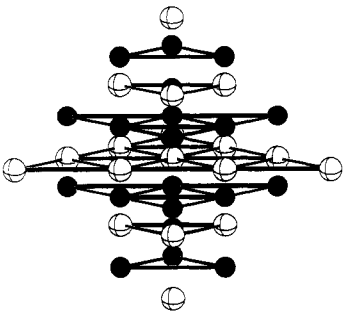

15

cut from the solid, modified by this insertion based on a related structure, is now complete.

To model a cluster, we assigned an H^- ligand to all Ni atoms that lie on the 12 apices of the 4 triangular nickel layers (see **16**).

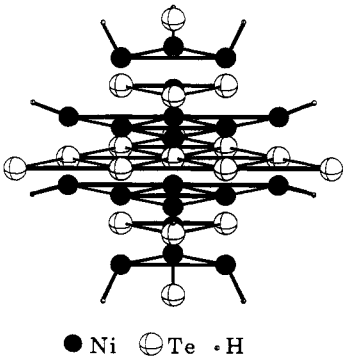

16

The atoms must move substantially from the cut of the solid to the $[Ni_{20}Te_{18}H_{12}]^{12-}$ cluster. To retain D_3 symmetry at Te_c, all sets of atoms will rotate around the central C_3 axis. The outermost Ni triangular planes must attain a staggered position with respect to each other. Finally, all neighboring planes of either Ni or Te atoms will be successively staggered (see **17**, the cluster redrawn in a way to emphasize the relationship to the cut).

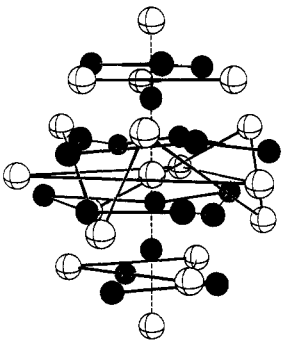

17

Comparing **15** and **17**, we notice that Ni atoms move in a way that can be separated into two components. First, the nickel triangles rotate around the principal C_3 axis of the system, giving a staggered conformation. Second, the Ni atoms move from the original hexagonal planes, alternately above and below, to reach staggered (chairlike) conformations. This motion is reminiscent of what transpires in the smaller Ni_9 cluster. All Ni–Ni intralayer contacts are 3.97 Å in the solid, whereas in the cluster, the Ni–Ni distances in the outermost Ni layers contract to approximately 3.8 Å. In the "chairs", there are six Ni–Ni bonds (2.7 Å) and six more Ni–Ni separations (4.05 Å).

The most dramatic movement toward the chair conformation is that of the six Te atoms surrounding the central Te_c. The hexagon they form in the cut has a side of 3.97 Å, and the irregular chain they form in the cluster has alternately long and short sides of 6.56 and 3.38 Å on the average. The three Te atoms defining the positions of the three 2-fold axes move closer to Te_c from a distance of 6.87 to 4.51 Å, without departing from their initial plane.

Finally, along the principal axis of the molecule, the outermost, capping Te atoms move toward Te_c, from a distance of 5.36 Å

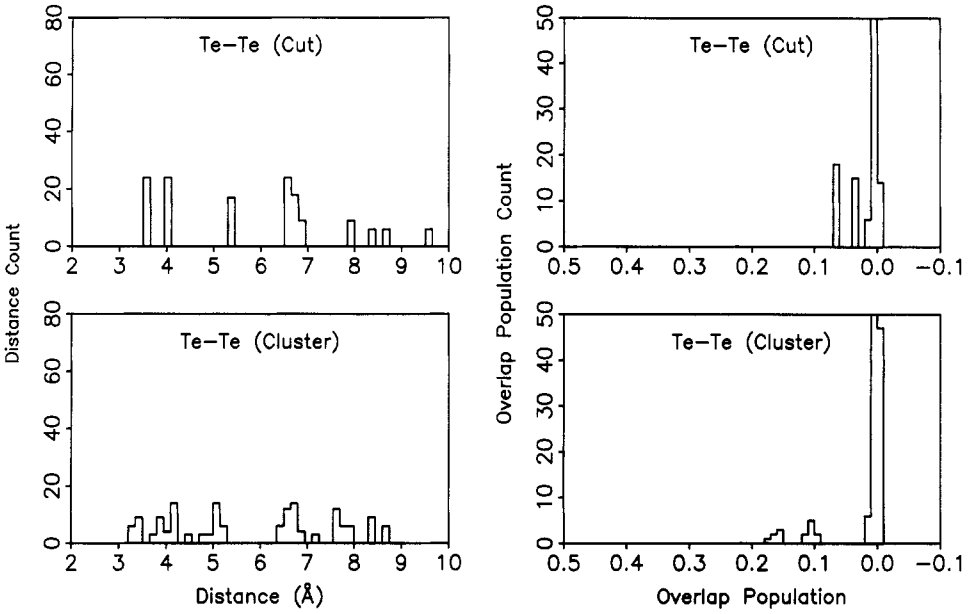

Figure 6. Distribution of Te–Te separations and of their associated reduced overlap populations in the cut and cluster models of the $Ni_{20}Te_{18}$ fragment. The number of Te–Te reduced overlap populations near zero for both configurations is very large, off scale in these graphs. We chose to truncate the peak around zero overlap population since such values do not contribute to the stability of the two systems.

in the solid to 5.10 Å in the cluster. The Ni_c-type atoms also move closer to the central Te atom from the initial NiTe interlayer distance of 2.68 Å to approximately 2.52 Å.

During the transit of the atoms in the model of a piece of solid we constructed to the final configuration of the $[Ni_{20}Te_{18}H_{12}]^{12-}$ model cluster, there is much going on, a flavor of which we tried to give above. We will conclude it with some calculational results. The total energy of the $[Ni_{20}Te_{18}H_{12}]^{12-}$ cluster, a model for the $[Ni_{20}Te_{18}(PEt_3)_{12}]$ cluster, was calculated. It turns out that the configuration of the cluster is indeed more stable than the corresponding configuration of the solid, by at least 8 eV.

What Makes the Cluster Rearrange from the Cut?

In order to trace and present more clearly the factors responsible for the stabilization of the model cluster $[Ni_{20}Te_{18}H_{12}]^{12-}$ over the corresponding solid, we plotted a distance distribution of all of the Ni–Ni, Ni–Te, and Te–Te bonds for the two systems, as well as a distribution of their associated overlap populations.

For the three different types of interatomic distances, we counted the number that lie within intervals of 0.15 Å, in the range of distance values 2.0–10.0 Å, for both the cut and the cluster. The histograms of Figures 4–6 show quite distinct peaks for the solid NiTe, a distribution terminated due to the finite size of the "cut" that we isolated. The corresponding histograms for the cluster have much broadened peaks. For the subsets of Ni and Te atoms, separately (Figures 4 and 6), it seems that the broadened distance distribution peaks in the cluster are centered around the corresponding peaks in the cut. *This convinces us that the subsets of the two different types of atoms are structurally very similar in the cluster and in bulk NiTe.*

This is not the case for the distribution of the Ni–Te bond lengths (see Figure 5). For the cluster, the peaks are broadened quite substantially and shifted toward the central region of 4–7 Å. This distribution is quite different from that of the solid. There is much stabilization to be gained in the Ni–Te bonds, so these distances adjust most to the process of cutting out a chunk of the solid.

We have also plotted a distribution of the reduced overlap populations of the three types of bonds in the two systems. We counted the number of populations that lie within intervals of 0.01 in the range of populations −0.10 to +0.50. Here again, the peaks for the cluster are a little broadened, around the corresponding distinct values for the cut, for all Ni–Ni and Te–Te contacts (see Figures 4 and 6). As a result, they give rise to peaks at higher values of overlap population, which did not exist in the cut. An example are two significantly bonding Te–Te peaks emerging in the 0.09–0.18 region, supporting the assumption that enhancement of Te–Te bonding does play a significant role in the stabilization of the cluster over the cut. Similarly, for the Ni–Ni overlap populations, nine values appear in the 0.07–0.09 region, again stabilizing the cluster over the cut.

The Ni–Te overlap populations follow the Ni–Te distance distribution (Figure 5). There are broad peaks here as well, shifted substantially toward higher values of overlap population. The 12 strongest Ni–Te bonds in the cluster are characterized by an overlap population value range of 0.40–0.43, whereas the strongest such bonds in the cut have an overlap population value of 0.40 (6 of them in our specific cut). We conclude from this analysis that the Ni and Te subsets from the solid NiTe are structurally rearranged, by motion of one sublattice with respect to the other,

Table II. Electron Occupation (%) of the Three Near-HOMO Levels in the $[Ni_{20}Te_{18}H_{12}]^{12-}$ Cluster

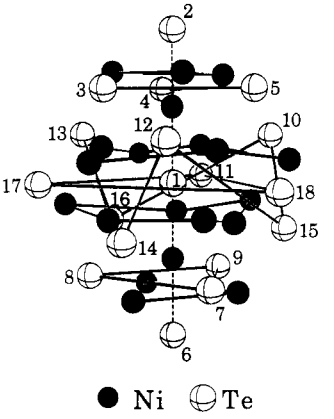

atom types	group total	single atom
Te(1)	2.5	2.5
Te(2,6)	4.5	2.2
Te(3,4,5,7,8,9)	11.2	1.9
Te(11,17,18)	18.2	6.1
Te(10,12,13,14,15,16)	9.0	1.5
Ni_c	6.0	3.0
Ni_b	16.9	2.8
Ni_a	22.2	1.8
H's	9.4	0.8
sum for all three MO's	100.0	

Table III. Parameters Used in the Extended Hückel Calculations

atom	orbital	H_{ii}, eV	ζ_1	ζ_2	C_1[a]	C_2[a]
Ni	3d	−14.20	5.75	2.30	0.5798	0.5782
	4s	−10.95	2.10			
	4p	−6.27	2.10			
Te	5s	−20.78	2.51			
	5p	−13.20	2.16			
H	1s	−13.60	1.30			

[a] Coefficients used in the double-ζ expansion of the d orbitals.

to yield a more stable system, the $Ni_{20}Te_{18}L_{12}$ cluster, and that the driving force for reconstruction is the formation of stronger Ni–Te bonds.

We conclude our discussion of the $Ni_{20}Te_{18}(PEt_3)_{12}$ cluster by commenting on its magnetic properties. Schneemeyer et al.[13] measured the magnetic susceptibility of this compound as a function of temperature. They reported that this cluster is paramagnetic, obeying the Curie–Weiss law, with a susceptibility roughly equal to that of two unpaired electrons.

Our calculations for the model $[Ni_{20}Te_{18}H_{12}]^{12-}$ cluster result in a HOMO–LUMO gap of only 0.06 eV. There is another level only 0.01 eV below the HOMO, and one 0.23 eV above the LUMO. Grouping the HOMO, next-HOMO, and LUMO together (all within 0.07 eV of each other) and filling these with four electrons, we can account for the magnetism. Trying to recognize which atoms are responsible for the paramagnetism of the whole cluster, we found that 6% of the above-mentioned three levels is to be found on each of three symmetry-related Te atoms in the cluster, the three telluriums that lie in the same plane with Te_c in **17** (Te11, Te17, and Te18 in Table II). In Table II we report the electron density on different groups of equivalent atoms, as well as on individual atoms. This is done for four electrons which actually occupy these nearly degenerate levels. It may be seen that the electron density in these MO's is about equally split between nickel and tellurium atoms.

The fact that there is such a high density of states at the "Fermi level" of the cluster is remarkable and indicates that $Ni_{20}Te_{18}(PEt_3)_{12}$ is a small fragment of a metal.

Summary

We have traced possible structural relationships between two molecular clusters of Ni and Te and the geometry of bulk NiTe. The calculations on the small Ni_9Te_6 cluster lead to the conclusion that a geometry partway between the observed cluster and the solid might be enthalpically favored. There is a conceptually clear pathway between the cluster observed and the corresponding cut from the solid. Some atoms move a great deal, others less so—the driving force seems to be a maximization of Ni–Te bonding.

The structure of the larger $Ni_{20}Te_{18}$ cluster at first seems unrelated to that of bulk NiTe. But a careful analysis reveals trios of Ni and Te atoms which can be related to the bulk structure by relatively small and systematic rotations. In this way all the Te atoms and 18 of the 20 nickel atoms can be accounted for. Each of the remaining Ni atoms enters an interstitial site in a trigonal prism of Ni atoms, just as they do in a "filled" NiAs structure, that of Ni_2In.

We stress here that this study of structural relationships between the Ni_9Te_6, $Ni_{20}Te_{18}$ clusters and the NiTe solid is not exhaustive, nor are the pathways we show uniquely defined. As a reviewer correctly remarked, the distortions we envisage are thought experiments; the real mechanism of NiTe formation is likely to involve heterogeneous decomposition or polymerization of the clusters on a surface.

We hope this is only the beginning of a methodical correlation of molecular clusters to extended structures, as we improve our understanding of the evolution of the size-dependent properties.

Acknowledgment. We are grateful to the National Science Foundation for its support of this work through Research Grants CHE-8912070 and DMR-8818558. Z.N. especially thanks Yuri Slovokhotov for his help through long, insightful discussions. B.S. thanks the Deutscher Akademischer Austauschdienst for the award of a NATO postdoctoral fellowship. We also thank D. W. Murphy, L. F. Schneemeyer, J. V. Waszczak, T. Palstra, A. Ramirez, and E. M. Gyorgy for stimulating discussions.

Appendix

The extended Hückel method[17] was used for all the calculations. Parameters are listed in Table III. The values of these parameters were taken from previously published work.[11]

(17) (a) Hoffmann, R.; Lipscomb, W. N. *J. Chem. Phys.* **1962**, *37*, 2872. (b) Hoffmann, R. *J. Chem. Phys.* **1963**, *39*, 1397.